

Geophysical Research Letters

RESEARCH LETTER

10.1029/2018GL080770

Key Points:

- In Hurricane Harvey's eyewall, polarimetric radar variables show azimuthally shifted wavenumber-1 asymmetric structures associated with the environmental vertical wind shear
- The variation of the raindrop size distribution within Harvey's eyewall is associated with the environmental vertical wind shear and size sorting processes
- The microphysical characteristics can be applied to evaluate forecasts and to improve microphysical parameterization in numerical weather prediction models

Correspondence to:

Y.-C. Feng,
yacfeng@rams.colostate.edu

Citation:

Feng, Y.-C., & Bell, M. (2019). Microphysical characteristics of an asymmetric eyewall in major Hurricane Harvey (2017). *Geophysical Research Letters*, 46, 461–471. <https://doi.org/10.1029/2018GL080770>


Received 3 OCT 2018

Accepted 14 DEC 2018

Accepted article online 26 DEC 2018

Published online 10 JAN 2019

Microphysical Characteristics of an Asymmetric Eyewall in Major Hurricane Harvey (2017)

Ya-Chien Feng¹  and Michael M. Bell¹ 

¹Department of Atmospheric Science, Colorado State University, Fort Collins, CO, USA

Abstract Microphysical and kinematic structures of major Hurricane Harvey's (2017) asymmetric eyewall are analyzed from ground-based polarimetric and airborne Doppler radars. New polarimetric observations of differential reflectivity (Z_{DR}) and specific differential phase (K_{DP}) show asymmetric wavenumber-1 patterns associated with vertical wind shear (VWS) but were shifted azimuthally with respect to the reflectivity (Z_H) asymmetry. A Z_{DR} column was found upwind of the Z_H maximum in a region with strong updrafts estimated from multi-Doppler synthesis, with higher values of K_{DP} found cyclonically downwind. Retrieved raindrop size distributions show that azimuthal variations of size and number concentration were determined by both the VWS and the size sorting process. The diameter of raindrops decreases, while the number concentration increases cyclonically downwind of VWS-induced updrafts due to the differential terminal fall speed of raindrops and strong rotational flow at major hurricane wind speeds.

Plain Language Summary Hurricane forecasts are highly sensitive to the representation of raindrop properties in numerical weather prediction models. Hurricane Harvey (2017) was the first major hurricane of category 4 intensity to make U.S. landfall since the recent upgrade of the U.S. weather radar network to dual-polarization technology that allows for better characterization of the shape, size, and number of raindrops in hurricanes. These new observations indicate substantial variation in the raindrop size distribution around Harvey's intense, asymmetric eyewall. Through additional analysis of data collected by the airborne Hurricane Hunters, we find that the largest raindrops are located where upward motion occurs due to interactions of environmental wind shear and strong rotational winds. The diameter of raindrops decreases, but the number of raindrops increases downwind of the updrafts around the eyewall. This new analysis can be used to evaluate and improve numerical models used in hurricane forecasting.

1. Introduction

Microphysical processes within tropical cyclones (TCs) play a critical role in determining structure, track, and intensity through their interaction with the storm dynamics. Numerical weather prediction (NWP) TC forecasts are highly sensitive to microphysical parameterization schemes due to these complex, multiscale interactions (Fovell et al., 2009; Jin et al., 2014; Khain et al., 2016; McFarquhar & Black, 2004; McFarquhar et al., 2006; Pattnaik et al., 2010; Tao et al., 2011). Interactions between environmental vertical wind shear (VWS), convective organization, and microphysical processes make forecasts of intensity change particularly difficult, with relatively slow progress compared to track forecasts (DeMaria et al., 2014). The recent upgrade of the U.S. operational radar network to dual polarization has provided new opportunities to gain insights on the bulk microphysical characteristics of TCs (Brown et al., 2016; Didlake & Kumjian, 2017; Griffin et al., 2014; Kalina et al., 2017), but many unknowns remain. In this study, new dual-polarization radar observations of Hurricane Harvey (2017) are analyzed to provide one of the first looks at the raindrop size distributions (DSD) and the microphysical processes in the eyewall of a major hurricane (>50 m/s).

Dual-polarization radars obtain backscattering information of hydrometeors from both horizontal and vertical polarizations (Seliga & Bringi, 1976). Bulk microphysical information about the type, shape, size, and quantity of hydrometeors within the sampling volume is provided (Bringi & Chandrasekar, 2001; Vivekanandan et al., 1999). Dual-polarization radars have been used to study microphysical characteristics for continental weather phenomena for many years, but there have been very few observations of TCs

until recently. May et al. (2008) first used dual-polarization radar variables and hydrometeor classification method to investigate the hydrometeor distribution in TC Ingrid. Chang et al. (2009) performed a combined disdrometer and polarimetric radar analysis to retrieve the DSD in TC rainbands and found an average mass-weighted diameter of about 2 mm and a normalized intercept of about $10^{3.8} \text{ mm}^{-1} \text{ m}^{-3}$, which is a maritime-like convective-type DSD (Bringi et al., 2003). The characteristic DSD of high concentrations of small raindrops in a TC was consistent with earlier in situ observations from airborne probes (Jorgensen & Willis, 1982) and surface disdrometers (Tokay et al., 2008; Ulbrich & Lee, 2002; Wilson & Pollock, 1974). Brown et al. (2016) used radar observations to identify model deficiencies in representing TC DSDs, resulting in improvements to the representation of the snow melting process in the Thompson-Eidhammer microphysical scheme (Brown et al., 2017). The DSD variation in TC rainbands (Wang et al., 2016, 2018; Wen et al., 2018) and variability in ice distributions (Didlake & Kumjian, 2017; Kalina et al., 2017) have also been recently investigated.

The majority of DSD observations in previous studies come from TC rainbands due to their prevalence and easier in situ sampling than the eyewall where the strongest winds are located. While there are some previous microphysical observations in TC eyewalls, the number of samples in major hurricanes are very limited due to the rarity of the phenomena and difficulty in sampling. Hurricane Harvey (2017) was the first major hurricane landfall in the U.S. since Wilma (2005) and the first since the operational radar upgrade to dual polarization in 2013. Of particular interest to the current study is the influence of VWS on Harvey's eyewall structure prior to landfall, which introduced a strong asymmetry in the observed polarimetric variables. The asymmetric structure of hurricane eyewalls is a well-known response to VWS (Black et al., 2002; Corbosiero & Molinari, 2003; Marks & Houze, 1987) and is often associated with intensity change (Nguyen & Molinari, 2012; Reasor et al., 2009; Rogers et al., 2016). The low-level convergence and upward motion mostly occur in the downshear direction, where abundant hydrometeors are generated and then advected downwind to the left of the shear vector, where the reflectivity maximum is frequently observed (Black et al., 2002; DeHart et al., 2014; Foerster et al., 2014; Hencé & Houze, 2011; Reasor et al., 2013; Tao et al., 2017). The dynamical interaction between the vortex and VWS to produce the eyewall asymmetry has been well studied (Frank & Ritchie, 2001; Jones, 1995; Reasor et al., 2004; Riemer et al., 2010, 2013), but the microphysical characteristics and their effect on eyewall structure are not well understood.

In the current study, polarimetric radar observations are used to document the microphysical asymmetries in Hurricane Harvey's eyewall and retrieve the rain DSDs in a major hurricane impacted by VWS. The results suggest that the interaction between asymmetric dynamical forcing of vertical motion and the differential terminal fall speed of raindrops in a strongly rotating environment plays an important role in producing the observed polarimetric signatures. The results not only have important implications for our fundamental understanding of microphysical and dynamic interactions in TCs but also provide constraints for NWP where overestimation or underestimation of the raindrop size can have a significant impact on the intensity and accumulated rainfall of the simulated TC (Brown et al., 2016; Tao et al., 2011). The data and methods are presented in section 2, followed by the results of the polarimetric analysis in section 3. A summary of the key findings in section 4.

2. Data and Methods

Hurricane Harvey (2017) was a category 4 hurricane in the Atlantic basin that brought significant rainfall to the Texas coast and caused severe social and economic losses (Blake & Zelinsky, 2017). Figure 1 shows the hurricane track and intensity and environmental VWS. Rapid intensification started on 25 August, and the hurricane center made landfall in San Jose Island, Texas, at 03 UTC on 26 August with 59-m/s (115 kt) winds and a minimum central pressure of 937 hPa. The mean storm motion was about 3–4 m/s to the northwest before landfall. The deep layer 200–850 hPa VWS vector was about 7 m/s (15 kt) from 220° to 270° . The main focus of this study is Harvey's asymmetric precipitation distribution due to VWS prior to landfall.

Data from the operational Weather Surveillance Doppler (WSR-88D) dual-polarization radar in Corpus Christi, Texas (KCRP), were analyzed from 23 UTC 25 August to 02 UTC 26 August when the hurricane center was within 100 km of the radar. In this study, we focus on three dual-polarimetric variables: reflectivity at horizontal polarization (Z_H), differential reflectivity (Z_{DR}), and specific differential phase (K_{DP}). Z_{DR} is the ratio between reflectivity at horizontal and vertical polarization, with higher positive values in rain

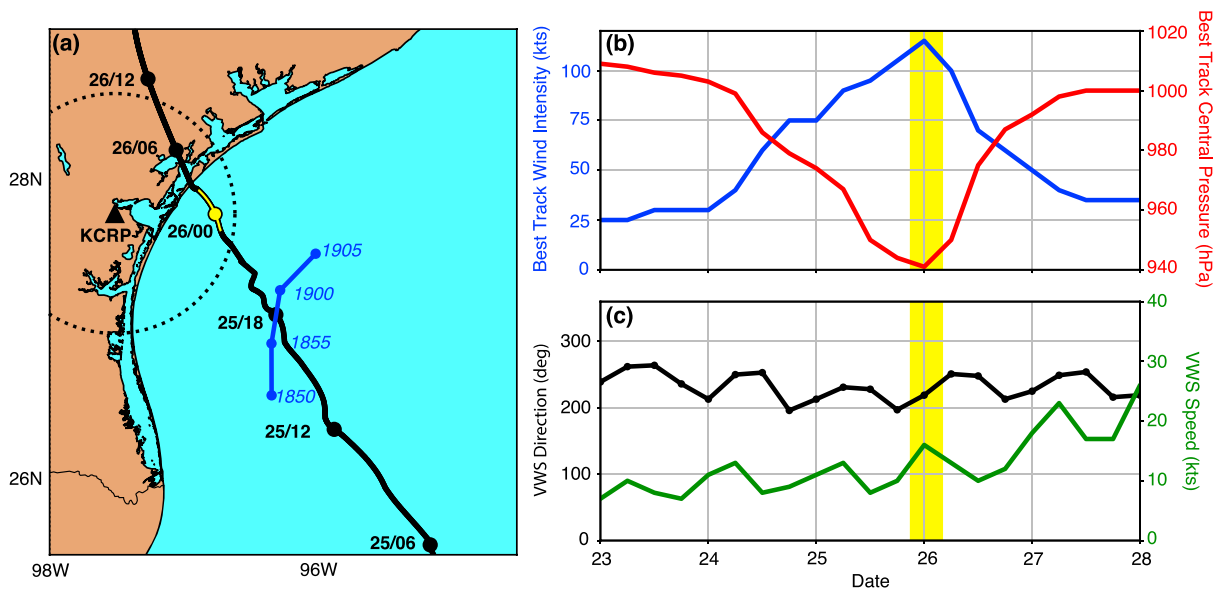


Figure 1. (a) High-resolution track of Hurricane Harvey from 25 to 26 August 2017 derived from aircraft in situ data courtesy NOAA Hurricane Research Division. The dotted circle indicates the 100-km range ring from the KCRP radar denoted by the triangle. Blue line is the track of NOAA P-3 from 1850 to 1905 UTC. Yellow line corresponds to the analysis period. (b) National Hurricane Center best track wind intensity (blue) and minimum central pressure (red). Yellow bar indicates analysis period. (c) Vertical wind shear direction (black) and speed (green) from the Statistical Hurricane Intensity Prediction Scheme (SHIPS) database (DeMaria et al., 2005). NOAA = National Oceanic and Atmospheric Administration; VWS = vertical wind shear.

indicative of larger oblate drops. K_{DP} is the range derivative of phase difference between horizontal and vertical polarization returns and is proportional to the number concentration of medium-sized (1–3 mm) oblate drops.

Several steps were taken to process the polarimetric radar data for quality control and microphysical analysis. Nonmeteorological returns were removed using a threshold of copolar correlation coefficient below 0.85. A Z_{DR} bias of -0.08 dB was corrected based on the algorithm of Cunningham et al. (2013). The Lidar Radar Open Software Environment (LRSOE) was used for K_{DP} calculation and radar data interpolation from spherical to Cartesian coordinates with vertical and horizontal resolution of 0.5- and 1-km spacing. For discussing the azimuthal variation of radar variables, we further interpolate the grid data into polar coordinates with the origin as the hurricane center and with the resolution of 1° azimuth \times 1-km radial distance. To describe the bulk rain DSD characteristics, the median volume diameter (D_0) and normalized intercept parameter (N_w , related to the number concentration) of a normalized gamma DSD were retrieved from Z_H and Z_{DR} based on Bringi et al. (2015) using the CSU_RadarTools software package.

The kinematic wind field was retrieved from P-3 airborne tail Doppler radar using the SAMURAI variational analysis technique as described in Foerster et al. (2014). One 15-min flight segment (Figure 1a) was analyzed to provide a quantitative measure of the tangential and vertical velocity. The airborne radar data were quality controlled using the “high” threshold automatic editing technique from Bell et al. (2013). Additional manual quality control was conducted to remove data near the aircraft due to poor data quality within 3-km range.

3. Results

Figure 2a shows the wavenumber-1 asymmetric precipitation pattern of Harvey’s eyewall. The highest Z_H values exceeding 40 dBZ at 1.5-km altitude were found to the left of the VWS vector. The eyewall Z_H asymmetric pattern associated with the VWS is broadly consistent with previous research of shear-induced asymmetric eyewall found both in numerical models (Braun, 2002; Rogers et al., 2003) and observations (Corbosiero et al., 2006; DeHart et al., 2014; Hence & Houze, 2011; Reasor et al., 2013). Though the moderate VWS is believed to be the dominant driver of the asymmetry, the effects from storm motion (Shapiro, 1983) and land interactions (Didlake & Kumjian, 2017) may also play a role in enhanced Z_H in the upshear left quadrant.

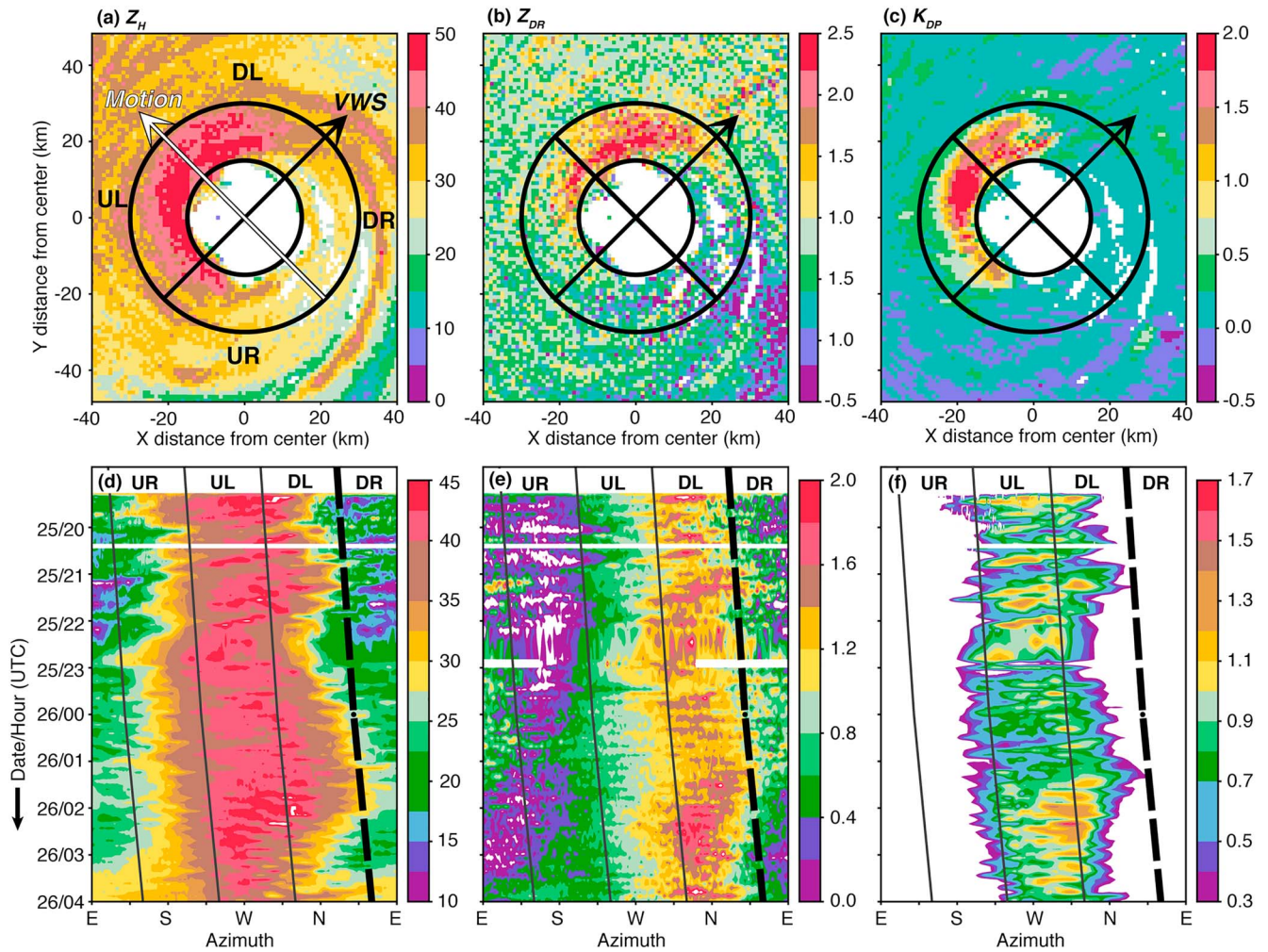


Figure 2. Harvey's eyewall (a) reflectivity Z_H (dBZ), (b) differential reflectivity Z_{DR} (dB), and (c) specific differential phase K_{DP} ($^{\circ}\text{km}^{-1}$) at 1.5-km height at 02 UTC 26 August. Black arrow indicates the vertical wind shear vector (VWS), with four quadrants denoting downshear left (DL), upshear left (UL), upshear right (UR), and downshear right (DR). The white arrow indicates the approximate storm motion direction. (d–f) Azimuth-time plots of Z_H , Z_{DR} , and K_{DP} fields averaged 15–30 km from the eyewall center at 1.5-km height. Shear-related quadrants are denoted, and thick dashed line indicates the downshear direction.

The polarimetric radar observations show that Z_{DR} and K_{DP} fields (Figures 2b and 2c) have wavenumber-1 eyewall asymmetric structures that are azimuthally shifted relative to Z_H . Higher values of Z_{DR} are found cyclonically upwind of the maximum of wavenumber-1 Z_H pattern, but higher values of K_{DP} occurred cyclonically downwind of the high Z_{DR} areas. The radar signature suggests that relatively large raindrops with higher Z_{DR} values are present upwind of the asymmetric eyewall structure typically observed by Z_H alone. Following the TC circulation, an area of maximum K_{DP} and Z_H but with decreasing Z_{DR} value indicates an increasing number of smaller drops downwind of the Z_{DR} maximum.

To further analyze the asymmetry, the data were separated into four quadrants relative to the environmental VWS: downshear right (DR), downshear left (DL), upshear left (UL), and upshear right (UR). The azimuthal location of the polarimetric variables in the azimuth-time diagrams (Figures 2d–2f) is similar to the polar depiction shown in Figures 2a–2c, but the shear quadrants rotate in azimuth as the VWS vector rotates. The wavenumber-1 asymmetric patterns of Z_H , Z_{DR} , and K_{DP} fields are persistent for more than 8 hr during Hurricane Harvey's intensifying period before landfall at 03 UTC 26 August. The maximum wavenumber-1 Z_H pattern consistently extends from the DL to UL quadrants, while the high Z_{DR} values (>1.5 dB) are consistently found in the DL quadrant upwind of the wavenumber-1 Z_H asymmetry. About 60° in azimuth downwind of the Z_{DR} peak, the maximum K_{DP} with values $>1.5^{\circ}/\text{km}$ is consistently present. The high K_{DP} area is found downwind of DL quadrant into the UL quadrant, even as the azimuth that defines each quadrant changes.

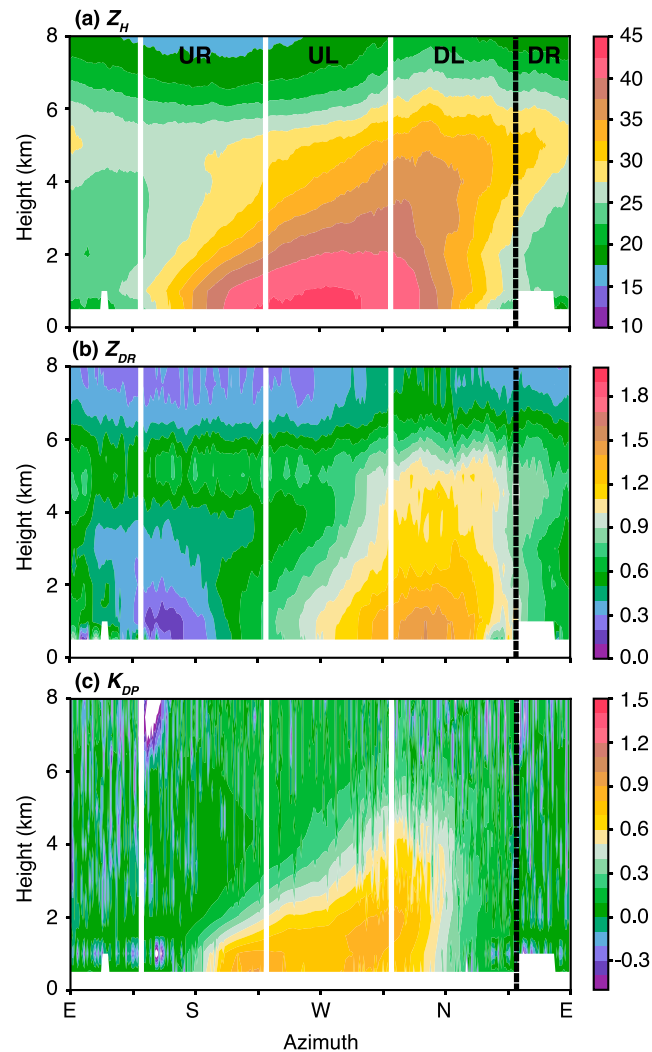


Figure 3. Azimuth-height plots of (a) Z_H (dBZ), (b) Z_{DR} (dB), and (c) K_{DP} ($^{\circ}\text{km}^{-1}$) averaged in 15- to 30-km radial from the eyewall during 23 UTC 25 August to 02 UTC 26 August. UR = upshear right; UL = upshear left; DL = downshear left; DR = downshear right.

Variations of polarimetric variables suggest the propagation and evolution of convective cells in the eyewall (Figures 2d–2f). In the DR quadrant, relatively low values of Z_H , Z_{DR} , and K_{DP} were found in the region where convection was initiated, followed by the maximum values in Z_{DR} as raindrops grow rapidly in the DL quadrant. Following the cyclonic flow downwind, Z_H and K_{DP} continue to increase in magnitude as the convection matures and raindrops are advected with the swirling wind. Embedded within the general wavenumber-1 convective evolution, there is substantial variation at higher wavenumbers of smaller-scale convective features that appear to propagate cyclonically downwind.

Figure 3 illustrates the temporally averaged azimuth-height structures of polarimetric variables in the eyewall. The peak values of Z_{DR} and Z_H are found at the lowest levels in the DL and UL quadrants, respectively. The 35-dBZ Z_H contour (Figure 3a) reaches its highest altitude in the DL quadrant, and the echo height slopes downward in the cyclonic direction. Higher values of Z_{DR} are mostly found to the DL quadrant, with values >1 dB extending to the melting level (~ 5 km). The Z_{DR} field (Figure 3b) also shows a melting level signature starting in the UL quadrant. The K_{DP} field has a vertical structure more similar to the Z_H field. Higher values of K_{DP} extend up just past the melting level in the DL quadrant, with the maximum downwind at lower levels into the UR quadrant.

The vertical microphysical structure and the distribution of hydrometeors are strongly related to the kinematic fields. Figure 4 shows dual-Doppler wind analysis of vertical velocity and horizontal wind speed from

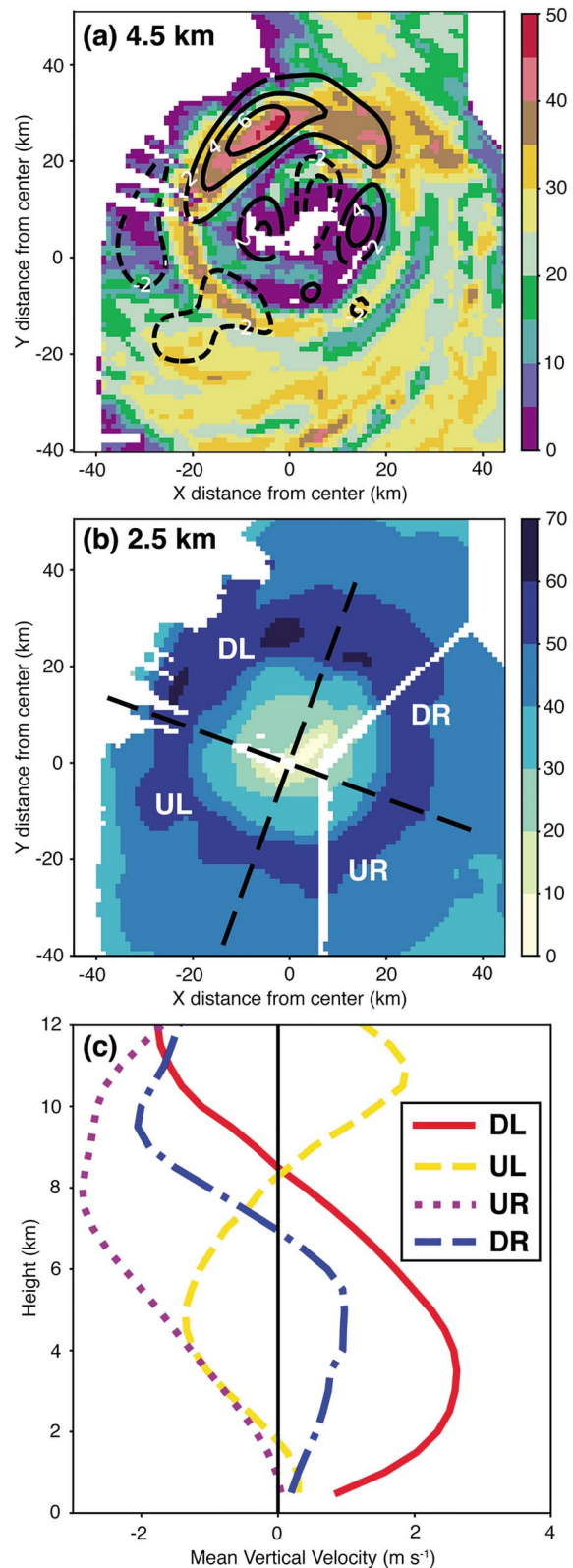


Figure 4. Kinematic fields from the airborne Doppler synthesis around 19 UTC 25 August. (a) Vertical velocity (m/s, contoured) overlaid on Z_H (dBZ, shaded) at 4.5-km height. (b) Horizontal wind speed (m/s) at 2.5-km height. The white data gap is along the flight path of the P-3 aircraft. (c) Average profiles of vertical velocity between 15 and 25 km radial distance in the four shear quadrants. UR = upshear right; UL = upshear left; DL = downshear left; DR = downshear right.

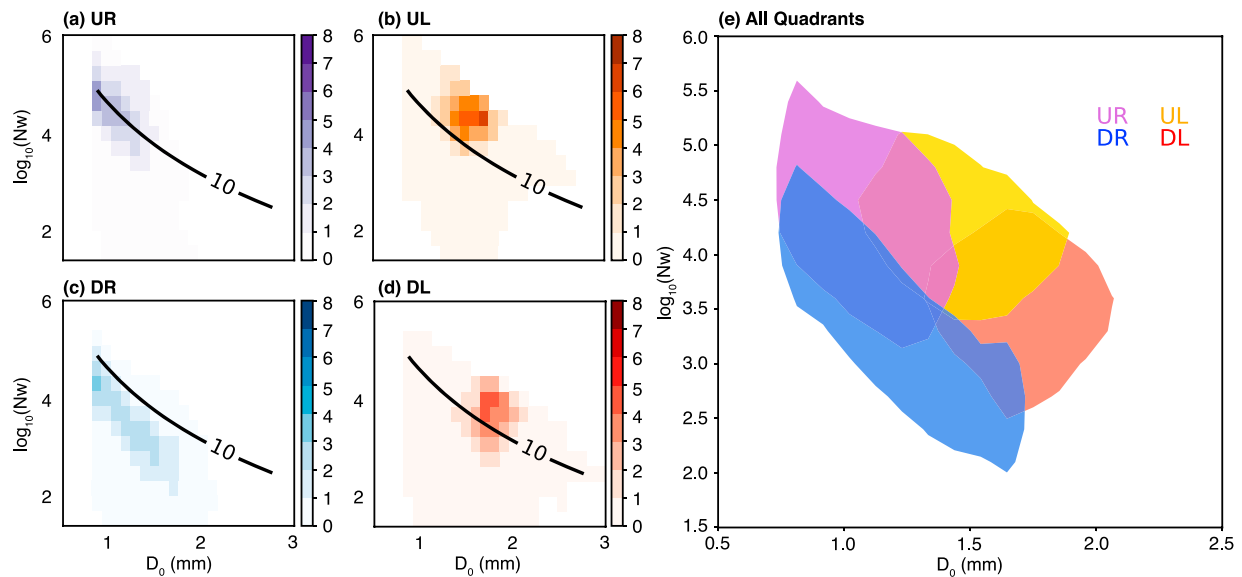


Figure 5. (a–d) Probability density frequency (% , shaded) of median volume diameter (D_0 , mm) and logarithmic normalized intercept parameter (N_w , $\log_{10} \text{mm}^{-1} \text{m}^{-3}$) of raindrops in shear relative quadrants. The probability distribution frequency is calculated from data within 15- to 30-km radius from the eyewall at 1.5-km height during 23 UTC 25 August to 02 UTC 26 August. The black line shows the corresponding rainfall rate equal to 10 mm/hr. (e) A summary figure of the variation of DSD in different shear relative quadrants: DL (red), UL (yellow), UR (purple) and DR (blue). Shading indicates probability distribution frequency greater than 1%.

the P-3 flight around 19 UTC. Though there was some slow evolution in the TC intensity, asymmetric structure, and VWS direction over the 9-hr analysis period, we can qualitatively interpret the Doppler-derived wind field as representative of the general kinematic structure during this period. The P-3 analysis shows that the strongest updrafts were found in the DL quadrant, consistent with the positive Z_{DR} column in this quadrant and previous airborne Doppler analyses of sheared eyewalls (DeHart et al., 2014; Foerster et al., 2014; Walder et al., 2018). Strong updrafts favor condensation of water vapor and the warm-rain collision-coalescence processes, which result in the size growth of hydrometeors (i.e., the increasing values of Z_{DR}). Positive Z_{DR} columns have also been found corresponding to the areas of convective updrafts in continental severe thunderstorms (Kumjian & Ryzhkov, 2008). The vertical velocity shows a maximum value near 6 m/s near 4 km in the DL quadrant (Figure 4a), and the average vertical motion was upward to 8-km altitude (Figure 4c). At 2.5 km, the intense wind speed exceeding 50 m/s (Figure 4b) rapidly advects falling hydrometeors generated in the updraft cyclonically around the vortex. In the UL quadrant, the average vertical motion was downward at low levels and upward aloft, consistent with the mass flux profile of stratiform precipitation. Predominately, downward vertical motion is seen in the UR quadrant, with correspondingly weaker reflectivity in the eyewall. The vertical profiles of polarimetric variables and vertical motion suggest a convective to stratiform transition cyclonically from the DR to UR quadrant, similar to that described by Foerster et al. (2014).

The azimuthal shift of the polarimetric variables indicates a spatial variation of DSD in the hurricane's asymmetric eyewall. Figure 5 demonstrates the joint probability distribution frequency of the median volume diameter (D_0) and the normalized intercept parameter (N_w) in four quadrants of VWS in the eyewall during the intensifying period. In Harvey's eyewall, the retrieved D_0 generally ranges from 0.7 to 2 mm and the N_w ranges from 10^2 to $10^{5.5} \text{mm}^{-1} \text{m}^{-3}$. Similar DSDs with a high concentration of small size drops have been reported in other TC observations (Chang et al., 2009; Tokay et al., 2008; Wang et al., 2016). The maximum drop size was observed in the DL quadrant but had a relatively low drop number concentration. Following the cyclonic eyewall circulation to the downwind quadrants, the average D_0 decreases as N_w increases. To the left of the VWS vector, less concentrations of large raindrops were found upwind but increasing concentrations of smaller raindrops were found downwind. The mean D_0 in the DL, UL, and UR quadrants are 1.7, 1.5, and 1 mm, respectively, and the mean N_w of these quadrants increases from $10^{3.7}$ to $10^{4.6} \text{mm}^{-1} \text{m}^{-3}$.

The cyclonic evolution of the retrieved DSD provides evidence of size sorting of raindrops. Size sorting occurs because of the differential sedimentation of hydrometeors with various sizes within the strong cyclonic

circulation. Smaller drops that fall with slower terminal velocities are advected farther than larger raindrops that fall faster from the same source region. We use a rough calculation to examine the fall trajectory of raindrops with different sizes in a simple vortex with a constant horizontal tangential wind equal to 50 m/s (similar to Figure 4b) neglecting vertical motion. Consider two raindrops with diameters of 1.2 mm ($Z_{DR} \sim 0.5$ dB, terminal velocity $V_t \sim 4.5$ m/s) and 2.2 mm ($Z_{DR} \sim 2$ dB, $V_t \sim 7$ m/s), continuously falling from 2 km to the ground. At a 25-km radius from the vortex center the small drop will travel 76° in azimuth, but the larger drop will only travel 50° in azimuth. The horizontal trajectory of larger raindrops is shorter than the smaller raindrops, thus having a significant effect on the observed polarimetric variables and inferred DSDs. Size sorting produces regions of sparsely concentrated large drops near the updraft region as the smaller drops are advected farther downwind, which contributes to the descending slopes in Z_H and K_{DP} fields and decreasing Z_{DR} from DL downwind to UR quadrants (Figure 3).

A summary figure (Figure 5e) shows a novel picture of how the DSDs vary around the asymmetric eyewall of a major hurricane due to the effects of VWS and size sorting. Even though the hurricane eyewall asymmetry has been documented in many studies using just the reflectivity field, the current study is believed to be the first to document the asymmetric DSDs and inferred microphysical processes in a major hurricane affected by VWS. Marks and Houze (1987) first discussed the size sorting of melting ice phase hydrometeors in the eyewall by calculating the hydrometeor trajectories from Z_H and the three-dimensional Doppler-derived wind field, but as demonstrated by the DSD retrieval, the combined Z_H and Z_{DR} fields provide more accurate information on hydrometeor sizes and associated terminal velocities compared with the Z_H field alone. The VWS-dependent DSD characteristics provide new evidence to build upon the results of Marks and Houze (1987) and demonstrate the size sorting effect in the TC asymmetric eyewall. While there are uncertainties in the absolute values of the DSD due to assumptions in the polarimetric retrieval algorithm, the relative changes in the DSD around the eyewall are much less sensitive to these assumptions and provide strong evidence for size sorting effect.

This study newly documents the azimuthal shift of Z_H and Z_{DR} in the TC eyewall, but similar localized updrafts and size sorting processes have been discussed in supercell thunderstorms (Dawson et al., 2014; Gunn & Marshall, 1955; Kumjian & Ryzhkov, 2012). The “ Z_{DR} arc” along the gradient in Z_H associated with size sorting is often present throughout the mature lifetime of supercell storms (Kumjian & Ryzhkov, 2008). For supercell convection, the polarimetric signatures are highly correlated with the low-level wind shear and have been applied for index of storm evolution for supercell cases (Kumjian & Ryzhkov, 2009). It remains to be seen whether the polarimetric signatures described here are common to many TCs or are a specific function of intensity and VWS and whether these signatures contain information about potential changes in TC intensity.

4. Summary

This research presents the polarimetric signatures and microphysical structure of rain in Hurricane Harvey's asymmetric eyewall at major hurricane intensity. The upgrade of the WSR-88D radar network to dual polarization prior to the landfalling category 4 hurricane provides an unprecedented look at the azimuthal variation of rain DSD due to environmental VWS and the size sorting process. During Harvey's intensifying period, an azimuthal wavenumber-1 asymmetric pattern in radar reflectivity (Z_H) was consistently observed on the left side of the environmental VWS direction for more than 8 hr. Within the maximum of the Z_H asymmetry, a maximum in differential reflectivity (Z_{DR}) persisted in the downshear left quadrant upwind of the Z_H maximum. The maximum specific differential phase (K_{DP}) was mostly collocated with the Z_H maximum but had a smaller extent downwind of the Z_{DR} maximum.

The radar-retrieved median volume diameter (D_0) and normalized intercept parameter (N_w) were quantitatively examined to demonstrate the spatial DSD variation of Hurricane Harvey's eyewall. A summary figure is proposed to illustrate the rain DSD characteristics of the asymmetric eyewall due to VWS and size sorting (Figure 5e). The highest D_0 was generally found in the DL quadrant and decreased cyclonically downwind while N_w increased. More collision-coalescence occur to produce larger size of raindrops in the region of the strongest updrafts, leading to higher Z_{DR} and D_0 in that region. A persistent Z_{DR} column vertically penetrating the melting level in the DL quadrant was in the same shear quadrant with the strongest updrafts in the eyewall calculated from airborne dual-Doppler wind synthesis. Larger raindrops with higher terminal velocity fall faster and result in a shorter horizontal propagation distance. The smaller raindrops with slower

terminal velocity are advected downwind by the TC's strong tangential winds and fall at farther distance. The results of this study suggest that the size sorting process and the variation of vertical motion induced by VWS play important roles to determine the azimuthal variability of rain DSDs and the surface precipitation pattern.

In ordinary precipitation, microphysical processes such as coalescence, breakup, and evaporation below the melting level can be identified by changes in 1-D vertical profiles of Z_H and Z_{DR} as “fingerprints” proposed by Kumjian and Prat (2014). However, the current results suggest that method is not sufficient to diagnose the microphysical processes in a TC eyewall. With complex shearing flows at high wind speeds, as well as an asymmetric distribution of vertical velocity, a more sophisticated model that considers the 3-D wind field is needed for better interpretation of the polarimetric signatures in the eyewall and infer more details about important processes. Further analysis of the evolving wind field from single Doppler retrievals could provide additional context for the polarimetric measurements and is a promising avenue for future research. The results of this study suggest that better understanding of asymmetries of the hurricane DSD can improve quantitative precipitation estimation and forecasting. Since NWP models can suffer from excessive size sorting (Igel et al., 2015; Khain et al., 2015), the rain DSD of the asymmetric eyewall documented in this study provides a useful metric for evaluating hurricane forecasts and improving model microphysical parameterization schemes. Further research to better understand how size sorting, collision-coalescence, and other microphysical processes evolve together with the dynamics and affect intensity change will be the subject of future work.

Acknowledgments

This work is supported by NSF awards AGS-1701225 and OAC-1661663 and ONR awards N000141613033 and N00014171223. The authors thank the suggestions from the anonymous reviewers and the discussion with the Bell research group and Brenda Dolan at CSU. The WSR-88D Level II radar data were obtained from the National Climatic Data Center (<https://www.ncdc.noaa.gov/nexradinv/>). NOAA P-3 radar data were obtained from the Hurricane Research Division (<http://www.aoml.noaa.gov/hrd/>). The LROSE software is available at <https://nsf-lrose.github.io/index.html>. The CSU RadarTools software is available at <https://github.com/CSU-Radarmet>.

References

- Bell, M. M., Lee, W.-C., Wolff, C. A., & Cai, H. (2013). A solo-based automated quality control algorithm for airborne tail doppler radar data. *Journal of Applied Meteorology and Climatology*, 52(11), 2509–2528. <https://doi.org/10.1175/JAMC-D-12-0283.1>
- Black, M. L., Gamache, J. F., Marks, F. D., Samsury, C. E., & Willoughby, H. E. (2002). Eastern Pacific Hurricanes Jimena of 1991 and Olivia of 1994: The effect of vertical shear on structure and intensity. *Monthly Weather Review*, 130(9), 2291–2312. [https://doi.org/10.1175/1520-0493\(2002\)130<2291:EPHJOA>2.0.CO;2](https://doi.org/10.1175/1520-0493(2002)130<2291:EPHJOA>2.0.CO;2)
- Blake, Eric S., & Zelinsky, D. A. (2017). Hurricane Harvey (al092017). Natl. Hurricane Cent., Miami, Fla.
- Braun, S. A. (2002). A cloud-resolving simulation of Hurricane Bob (1991): Storm structure and eyewall buoyancy. *Monthly Weather Review*, 130(6), 1573–1592. [https://doi.org/10.1175/1520-0493\(2002\)130<1573:ACRSOH>2.0.CO;2](https://doi.org/10.1175/1520-0493(2002)130<1573:ACRSOH>2.0.CO;2)
- Bringi, V. N., & Chandrasekar, V. (2001). *Polarimetric doppler weather radar: Principles and applications* (pp. 636). Cambridge, UK: Cambridge University Press.
- Bringi, V. N., Chandrasekar, V., Hubbert, J., Gorgucci, E., Randeu, W. L., & Schoenhuber, M. (2003). Raindrop size distribution in different climatic regimes from disdrometer and dual-polarized radar analysis. *Journal of the Atmospheric Sciences*, 60(2), 354–365. [https://doi.org/10.1175/1520-0469\(2003\)060<0354:RSDIDC>2.0.CO;2](https://doi.org/10.1175/1520-0469(2003)060<0354:RSDIDC>2.0.CO;2)
- Bringi, V. N., Tolstoy, L., Thurai, M., & Petersen, W. A. (2015). Estimation of spatial correlation of drop size distribution parameters and rain rate using NASA's S-band polarimetric radar and 2D video disdrometer network: Two case studies from MC3E. *Journal of Hydrometeorology*, 16(3), 1207–1221. <https://doi.org/10.1175/JHM-D-14-0204.1>
- Brown, B. R., Bell, M. M., & Frambach, A. J. (2016). Validation of simulated hurricane drop size distributions using polarimetric radar. *Geophysical Research Letters*, 43, 910–917. <https://doi.org/10.1002/2015GL067278>
- Brown, B. R., Bell, M. M., & Thompson, G. (2017). Improvements to the snow melting process in a partially double moment microphysics parameterization. *Journal of Advances in Modeling Earth Systems*, 9, 1150–1166. <https://doi.org/10.1002/2016MS000892>
- Chang, W.-Y., Wang, T.-C. C., & Lin, P.-L. (2009). Characteristics of the raindrop size distribution and drop shape relation in typhoon systems in the western Pacific from the 2D video disdrometer and NCU C-band polarimetric radar. *Journal of Atmospheric and Oceanic Technology*, 26(10), 1973–1993. <https://doi.org/10.1175/2009JTECHA1236.1>
- Corbosiero, K. L., & Molinari, J. (2003). The relationship between storm motion, vertical wind shear, and convective asymmetries in tropical cyclones. *Journal of the Atmospheric Sciences*, 60(2), 366–376. [https://doi.org/10.1175/1520-0469\(2003\)060<0366:TRBSMV>2.0.CO;2](https://doi.org/10.1175/1520-0469(2003)060<0366:TRBSMV>2.0.CO;2)
- Corbosiero, K. L., Molinari, J., Aiyyer, A. R., & Black, M. L. (2006). The structure and evolution of Hurricane Elena (1985). Part II: Convective asymmetries and evidence for vortex rossby waves. *Monthly Weather Review*, 134(11), 3073–3091. <https://doi.org/10.1175/MWR3250.1>
- Cunningham, J. G., Zittel, W. D., Lee, R. R., & Ice, R. L. (2013). Methods for identifying systematic differential reflectivity (Z_{DR}) biases on the operational WSR88D network, Paper presented at 36th Conference on Radar. Breckenridge, Colorado.
- Dawson, D. T., Mansell, E. R., & Kumjian, M. R. (2014). Does wind shear cause hydrometeor size sorting. *Journal of the Atmospheric Sciences*, 72(1), 340–348. <https://doi.org/10.1175/JAS-D-14-0084.1>
- DeHart, J. C., Houze, R. A., & Rogers, R. F. (2014). Quadrant distribution of tropical cyclone inner-core kinematics in relation to environmental shear. *Journal of the Atmospheric Sciences*, 71(7), 2713–2732. <https://doi.org/10.1175/JAS-D-13-0298.1>
- DeMaria, M., Mainelli, M., Shay, L. K., Knaff, J. A., & Kaplan, J. (2005). Further improvements to the statistical hurricane intensity prediction scheme (SHIPS). *Weather Forecasting*, 20(4), 531–543. <https://doi.org/10.1175/WAF862.1>
- DeMaria, M., Sampson, C. R., Knaff, J. A., & Musgrave, K. D. (2014). Is tropical cyclone intensity guidance improving? *Bulletin of the American Meteorological Society*, 95(3), 387–398. <https://doi.org/10.1175/BAMS-D-12-00240.1>
- Didlake, A. C. J., & Kumjian, M. R. (2017). Examining polarimetric radar observations of bulk microphysical structures and their relation to vortex kinematics in Hurricane Arthur (2014). *Monthly Weather Review*, 145(11), 4521–4541. <https://doi.org/10.1175/MWR-D-17-0035.1>
- Foerster, A. M., Bell, M. M., Harr, P. A., & Jones, S. C. (2014). Observations of the eyewall structure of Typhoon Sinlaku (2008) during the transformation stage of extratropical transition. *Monthly Weather Review*, 142(9), 3372–3392. <https://doi.org/10.1175/MWR-D-13-00313.1>

- Fovell, R. G., Corbosiero, K. L., & Kuo, H.-C. (2009). Cloud microphysics impact on hurricane track as revealed in idealized experiments. *Journal of the Atmospheric Sciences*, 66(6), 1764–1778. <https://doi.org/10.1175/2008JAS2874.1>
- Frank, W. M., & Ritchie, E. A. (2001). Effects of vertical wind shear on the intensity and structure of numerically simulated hurricanes. *Monthly Weather Review*, 129(9), 2249–2269. [https://doi.org/10.1175/1520-0493\(2001\)129<2249:EOVWSO>2.0.CO;2](https://doi.org/10.1175/1520-0493(2001)129<2249:EOVWSO>2.0.CO;2)
- Griffin, E. M., Schuur, T. J., MacGorman, D. R., Kumjian, M. R., & Fierro, A. O. (2014). An electrical and polarimetric analysis of the overland reintensification of Tropical Storm Erin (2007). *Monthly Weather Review*, 142(6), 2321–2344. <https://doi.org/10.1175/MWR-D-13-00360.1>
- Gunn, K. L. S., & Marshall, J. S. (1955). The effect of wind shear on falling precipitation. *Journal of Meteorology*, 12(4), 339–349. [https://doi.org/10.1175/1520-0469\(1955\)012<0339:TEOWSO>2.0.CO;2](https://doi.org/10.1175/1520-0469(1955)012<0339:TEOWSO>2.0.CO;2)
- Hence, D. A., & Houze, R. A. (2011). Vertical structure of hurricane eyewalls as seen by the TRMM precipitation radar. *Journal of the Atmospheric Sciences*, 68(8), 1637–1652. <https://doi.org/10.1175/2011JAS3578.1>
- Igel, A. L., Igel, M. R., & van den Heever, S. C. (2015). Make it a double? Sobering results from simulations using single-moment microphysics schemes. *Journal of the Atmospheric Sciences*, 72(2), 910–925. <https://doi.org/10.1175/JAS-D-14-0107.1>
- Jin, Y., Wang, S., Nachamkin, J., Doyle, J. D., Thompson, G., Grasso, L., et al. (2014). The impact of ice phase cloud parameterizations on tropical cyclone prediction. *Monthly Weather Review*, 142(2), 606–625. <https://doi.org/10.1175/MWR-D-13-00058.1>
- Jones, S. C. (1995). The evolution of vortices in vertical shear. I: Initially barotropic vortices. *Quarterly Journal of the Royal Meteorological Society*, 121(524), 821–851. <https://doi.org/10.1002/qj.49712152406>
- Jorgensen, D. P., & Willis, P. T. (1982). A Z-R relationship for hurricanes. *Journal of Applied Meteorology*, 21(3), 356–366. [https://doi.org/10.1175/1520-0450\(1982\)021<0356:AZRRFH>2.0.CO;2](https://doi.org/10.1175/1520-0450(1982)021<0356:AZRRFH>2.0.CO;2)
- Kalina, E. A., Matrosov, S. Y., Cione, J. J., Marks, F. D., Vivekanandan, J., Black, R. A., et al. (2017). The ice water paths of small and large ice species in Hurricanes Arthur (2014) and Irene (2011). *Journal of Applied Meteorology and Climatology*, 56(5), 1383–1404. <https://doi.org/10.1175/JAMC-D-16-0300.1>
- Khain, A. P., Beheng, K. D., Heymsfield, A., Korolev, A., Krichak, S. O., Levin, Z., et al. (2015). Representation of microphysical processes in cloud resolving models: Spectral (bin) microphysics versus bulk parameterization. *Reviews of Geophysics*, 53, 247–322. <https://doi.org/10.1002/2014RG000468>
- Khain, A., Lynn, B., & Shpund, J. (2016). High resolution WRF simulations of Hurricane Irene: Sensitivity to aerosols and choice of microphysical schemes. *Atmospheric Research*, 167, 129–145. <https://doi.org/10.1016/j.atmosres.2015.07.014>
- Kumjian, M. R., & Prat, O. P. (2014). The impact of raindrop collisional processes on the polarimetric radar variables. *Journal of the Atmospheric Sciences*, 71(8), 3052–3067. <https://doi.org/10.1175/JAS-D-13-0357.1>
- Kumjian, M. R., & Ryzhkov, A. V. (2008). Polarimetric signatures in supercell thunderstorms. *Journal of Applied Meteorology and Climatology*, 47(7), 1940–1961. <https://doi.org/10.1175/2007JAMC1874.1>
- Kumjian, M. R., & Ryzhkov, A. V. (2009). Storm-relative helicity revealed from polarimetric radar measurements. *Journal of the Atmospheric Sciences*, 66(3), 667–685. <https://doi.org/10.1175/2008JAS2815.1>
- Kumjian, M. R., & Ryzhkov, A. V. (2012). The impact of size sorting on the polarimetric radar variables. *Journal of the Atmospheric Sciences*, 69(6), 2042–2060. <https://doi.org/10.1175/JAS-D-11-0125.1>
- Marks, F. D., & Houze, R. A. (1987). Inner core structure of Hurricane Alicia from airborne Doppler radar observations. *Journal of the Atmospheric Sciences*, 44(9), 1296–1317. [https://doi.org/10.1175/1520-0469\(1987\)044<1296:ICSOHA>2.0.CO;2](https://doi.org/10.1175/1520-0469(1987)044<1296:ICSOHA>2.0.CO;2)
- May, P. T., Kepert, J. D., & Keenan, T. D. (2008). Polarimetric radar observations of the persistently asymmetric structure of tropical cyclone Ingrid. *Monthly Weather Review*, 136(2), 616–630. <https://doi.org/10.1175/2007MWR2077.1>
- McFarquhar, G. M., & Black, R. A. (2004). Observations of particle size and phase in tropical cyclones: Implications for mesoscale modeling of microphysical processes. *Journal of the Atmospheric Sciences*, 61(4), 422–439. [https://doi.org/10.1175/1520-0469\(2004\)061<0422:OOPSAP>2.0.CO;2](https://doi.org/10.1175/1520-0469(2004)061<0422:OOPSAP>2.0.CO;2)
- McFarquhar, G. M., Zhang, H., Heymsfield, G., Halverson, J. B., Hood, R., Dudhia, J., & Marks, F. (2006). Factors affecting the evolution of hurricane Erin (2001) and the distributions of hydrometeors: Role of microphysical processes. *Journal of the Atmospheric Sciences*, 63(1), 127–150. <https://doi.org/10.1175/JAS3590.1>
- Nguyen, L. T., & Molinari, J. (2012). Rapid intensification of a sheared, fast-moving hurricane over the gulf stream. *Monthly Weather Review*, 140(10), 3361–3378. <https://doi.org/10.1175/MWR-D-11-00293.1>
- Pattanaik, S., English, C., & Krishnamurti, T. N. (2010). Influence of rain-rate initialization, cloud microphysics, and cloud torques on hurricane intensity. *Monthly Weather Review*, 139(2), 627–649. <https://doi.org/10.1175/2010MWR3382.1>
- Reasor, P. D., Eastin, M. D., & Gamache, J. F. (2009). Rapidly intensifying Hurricane Guillermo (1997). Part I: Low-wavenumber structure and evolution. *Monthly Weather Review*, 137(2), 603–631. <https://doi.org/10.1175/2008MWR2487.1>
- Reasor, P. D., Montgomery, M. T., & Grasso, L. D. (2004). A new look at the problem of tropical cyclones in vertical shear flow: Vortex resiliency. *Journal of the Atmospheric Sciences*, 61(1), 3–22. [https://doi.org/10.1175/1520-0469\(2004\)061<0003:ANLATP>2.0.CO;2](https://doi.org/10.1175/1520-0469(2004)061<0003:ANLATP>2.0.CO;2)
- Reasor, P. D., Rogers, R., & Lorsolo, S. (2013). Environmental flow impacts on tropical cyclone structure diagnosed from airborne doppler radar composites. *Monthly Weather Review*, 141(9), 2949–2969. <https://doi.org/10.1175/MWR-D-12-00334.1>
- Riemer, M., Montgomery, M. T., & Nicholls, M. E. (2010). A new paradigm for intensity modification of tropical cyclones: Thermodynamic impact of vertical wind shear on the inflow layer. *Atmospheric Chemistry and Physics*, 10(7), 3163–3188. <https://doi.org/10.5194/acp-10-3163-2010>
- Riemer, M., Montgomery, M. T., & Nicholls, M. E. (2013). Further examination of the thermodynamic modification of the inflow layer of tropical cyclones by vertical wind shear. *Atmospheric Chemistry and Physics*, 13(1), 327–346. <https://doi.org/10.5194/acp-13-327-2013>
- Rogers, R., Chen, S., Tenerelli, J., & Willoughby, H. (2003). A numerical study of the impact of vertical shear on the distribution of rainfall in Hurricane Bonnie (1998). *Monthly Weather Review*, 131(8), 1577–1599. <https://doi.org/10.1175/2546.1>
- Rogers, R. F., Zhang, J. A., Zawislak, J., Jiang, H., Alvey, G. R., Zipser, E. J., & Stevenson, S. N. (2016). Observations of the structure and evolution of Hurricane Edouard (2014) during intensity change. Part II: Kinematic structure and the distribution of deep convection. *Monthly Weather Review*, 144, 3355–3376. <https://doi.org/10.1175/MWR-D-16-0017.1>
- Seliga, T. A., & Bringi, V. N. (1976). Potential use of radar differential reflectivity measurements at orthogonal polarizations for measuring precipitation. *Journal of Applied Meteorology*, 15(1), 69–76. [https://doi.org/10.1175/1520-0450\(1976\)015<0069:PUORDR>2.0.CO;2](https://doi.org/10.1175/1520-0450(1976)015<0069:PUORDR>2.0.CO;2)
- Shapiro, L. J. (1983). The asymmetric boundary layer flow under a translating hurricane. *Journal of the Atmospheric Sciences*, 40(8), 1984–1998. [https://doi.org/10.1175/1520-0469\(1983\)040<1984:TABLFU>2.0.CO;2](https://doi.org/10.1175/1520-0469(1983)040<1984:TABLFU>2.0.CO;2)
- Tao, C., Jiang, H., & Zawislak, J. (2017). The relative importance of stratiform and convective rainfall in rapidly intensifying tropical cyclones. *Monthly Weather Review*, 145, 795–809. <https://doi.org/10.1175/MWR-D-16-0316.1>
- Tao, W.-K., Shi, J. J., Chen, S. S., Lang, S., Lin, P.-L., Hong, S.-Y., et al. (2011). The impact of microphysical schemes on hurricane intensity and track. *Asia-Pacific Journal of Atmospheric Sciences*, 47(1), 1–16. <https://doi.org/10.1007/s13143-011-1001-z>

- Tokay, A., Bashor, P. G., Habib, E., & Kasparis, T. (2008). Raindrop size distribution measurements in tropical cyclones. *Monthly Weather Review*, *136*(5), 1669–1685. <https://doi.org/10.1175/2007MWR2122.1>
- Ulbrich, C. W., & Lee, L. G. (2002). Rainfall characteristics associated with the remnants of tropical storm Helene in upstate south Carolina. *Weather Forecasting*, *17*(6), 1257–1267. [https://doi.org/10.1175/1520-0434\(2002\)017<1257:RCAWTR>2.0.CO;2](https://doi.org/10.1175/1520-0434(2002)017<1257:RCAWTR>2.0.CO;2)
- Vivekanandan, J., Zrnich, D. S., Ellis, S. M., Oye, R., Ryzhkov, A. V., & Straka, J. (1999). Cloud microphysics retrieval using S-band dual-polarization radar measurements. *Bulletin of the American Meteorological Society*, *80*(3), 381–388. [https://doi.org/10.1175/1520-0477\(1999\)080<0381:CMRUSB>2.0.CO;2](https://doi.org/10.1175/1520-0477(1999)080<0381:CMRUSB>2.0.CO;2)
- Walder, J. B., Rogers, R. F., & Reasor, P. D. (2018). The relationship between spatial variations in the structure of convective bursts and tropical cyclone intensification as determined by airborne Doppler radar. *Monthly Weather Review*, *146*, 761–780. <https://doi.org/10.1175/MWR-D-17-0213.1>
- Wang, M., Zhao, K., Xue, M., Zhang, G., Liu, S., Wen, L., & Chen, G. (2016). Precipitation microphysics characteristics of a Typhoon Matmo (2014) rainband after landfall over eastern China based on polarimetric radar observations. *Journal of Geophysical Research: Atmospheres*, *121*, 12,415–12,433. <https://doi.org/10.1002/2016JD025307>
- Wen, L., Zhao, K., Wang, G., Zhou, B., Huang, H., Hu, D., et al. (2018). Drop size distribution characteristics of seven typhoons in China. *Journal of Geophysical Research: Atmospheres*, *123*, 6529–6548. <https://doi.org/10.1029/2017JD027950>
- Wilson, J. W., & Pollock, D. M. (1974). Rainfall measurements during Hurricane Agnes by three overlapping radars. *Journal of Applied Meteorology*, *13*(8), 835–844.